Supporting information for:

Dismantling the "Red Wall" of Colloidal Perovskites: Highly Luminescent Formamidinium and Formamidinium-Cesium Lead Iodide Nanocrystals

*Loredana Protesescu,[†,‡] Sergii Yakunin,[†,‡] Sudhir Kumar,[∥] Janine Bär,[†] Federica Bertolotti,[¥] Norberto Masciocchi,[¥] Antonietta Guagliardi,[¥,$] Matthias Grotevent,[†,§] Ivan Shorubalko,[§] Maryna I. Bodnarchuk,[†,‡] Chih-Jen Shih,[∥] and Maksym V. Kovalenko[†,‡]**

[†]Institute of Inorganic Chemistry, Department of Chemistry and Applied Bioscience, ETH Zürich, Vladimir Prelog Weg 1, CH-8093 Zürich, Switzerland

[‡]Laboratory for Thin Films and Photovoltaics, Empa – Swiss Federal Laboratories for Materials Science and Technology, Überlandstrasse 129, CH-8600 Dübendorf, Switzerland

[∥]Institute of Chemical and Bioengineering, Department of Chemistry and Applied Bioscience, ETH Zürich, Vladimir Prelog Weg 1, CH-8093 Zürich, Switzerland

[¥]Dipartimento di Scienza e Alta Tecnologia and To.Sca.Lab, Università dell'Insubria, via Valleggio 11, I-22100 Como, Italy

[$]Istituto di Cristallografia and To.Sca.Lab, Consiglio Nazionale delle Ricerche, Valleggio 11, I-22100 Como, Italy

[§]Laboratory for Reliability Science and Technology, Empa – Swiss Federal Laboratories for Materials Science and Technology, Überlandstrasse 129, CH-8600 Dübendorf, Switzerland

*mvkovalenko@ethz.ch

Table S1. The calculated tolerance and octahedral factors for the ABX_3 (A=Cs, MA, FA, B=Sn, Pb, X=I, Br, Cl) and the indication about their preferred structure at RT. The tolerance and octahedral factors were calculated using the radii from Table S2.

Compound (ABX_3)	Tolerance factor (**t**)	Octahedral factor (**μ**)	Known **stable** phases @ RT	Known **metastable** phases @ RT	Ref.
B=Pb					
$CsPbI_3$	0.89	0.47	1D	3D	*1, 2, 3, 4, 5, 6, 7, 8*
$CsPbBr_3$	0.92	0.50	1D	3D	*9, 10*
$CsPbCl_3$	0.93	0.54	3D		*9, 11, 12*
$MAPbI_3$	0.96	0.47	3D		*1, 13, 14*
$MAPbBr_3$	0.99	0.50	3D		*1, 13*
$MAPbCl_3$	1.00	0.54	3D		*13, 15*
$FAPbI_3$	1.04	0.47	1D	3D	*1, 2*
$FAPbBr_3$	1.08	0.50	3D		*9, 7, 16, 17, 18*
$FAPbCl_3$	1.09	0.54	3D		*19, 20*
B=Sn					
$CsSnI_3$	0.91	0.44	1D, 3D	3D	*21, 22, 23*
$CsSnBr_3$	0.94	0.48	3D		*23, 24*
$CsSnCl_3$	0.95	0.52	1D	3D	*23, 25, 26*
$MASnI_3$	0.97	0.44	3D		*5, 27, 28*
$MASnBr_3$	1.01	0.48	3D		*29, 30*
$MASnCl_3$	1.01	0.42	1D	3D	*30, 31*
$FASnI_3$	1.06	0.44	3D		*32, 33*
$FASnBr_3$	1.10	0.48	NA	NA	NA
$FASnCl_3$	1.10	0.42	NA	NA	NA

Table S2. The ionic radii used for the halide compounds (Shannon radii[34] for Cs^+, I^-, Br^-, Cl^-, and the revised radii from Travis *et al*.[35] for Pb^{2+}, Sn^{2+}, MA^+, FA^+).

Ion	**Ionic radius (Å)**		
6-coordinate B^{2+}	in iodides	in bromides	in chlorides
Pb^{2+}	1.03	0.98	0.99
Sn^{2+}	0.97	0.94	0.96
A cations			
Cs^+	1.88		
MA^+	2.16		
FA^+	2.53		
X anions			
I^-	2.2		
Br^-	1.96		
Cl^-	1.85		

Table S3. An overview of known $APbI_3$ (A= MA^+, Cs^+, FA^+) NCs with cubic or near cubic shapes.

Compound	**$MAPbI_3$ NCs (Ref.[36, 37])**	**$CsPbI_3$ NCs (Ref.[38])**	**$FA_{0.1}Cs_{0.9}PbI_3$ NCs** (this work)	**$FAPbI_3$ NCs** (this work)
Crystal structure	Tetragonal (I4cm)	3D-orthorhombic (pbnm)	3D-orthorhombic (pbnm)	α-cubic (pm3m)
Emission range	650 nm-750 nm	600-690 nm	680-690 nm	770-780 nm
PLQY	20-30 %	50-80%	>70 %	>70 %
Stability	less than 1 day after isolation and purification; several weeks when stored as a crude solution.	less than 1 day if purified and up to one week when stored as a crude solution.	several months in colloidal solution and up to few weeks in films.	Stable for months in colloidal solutions and films.

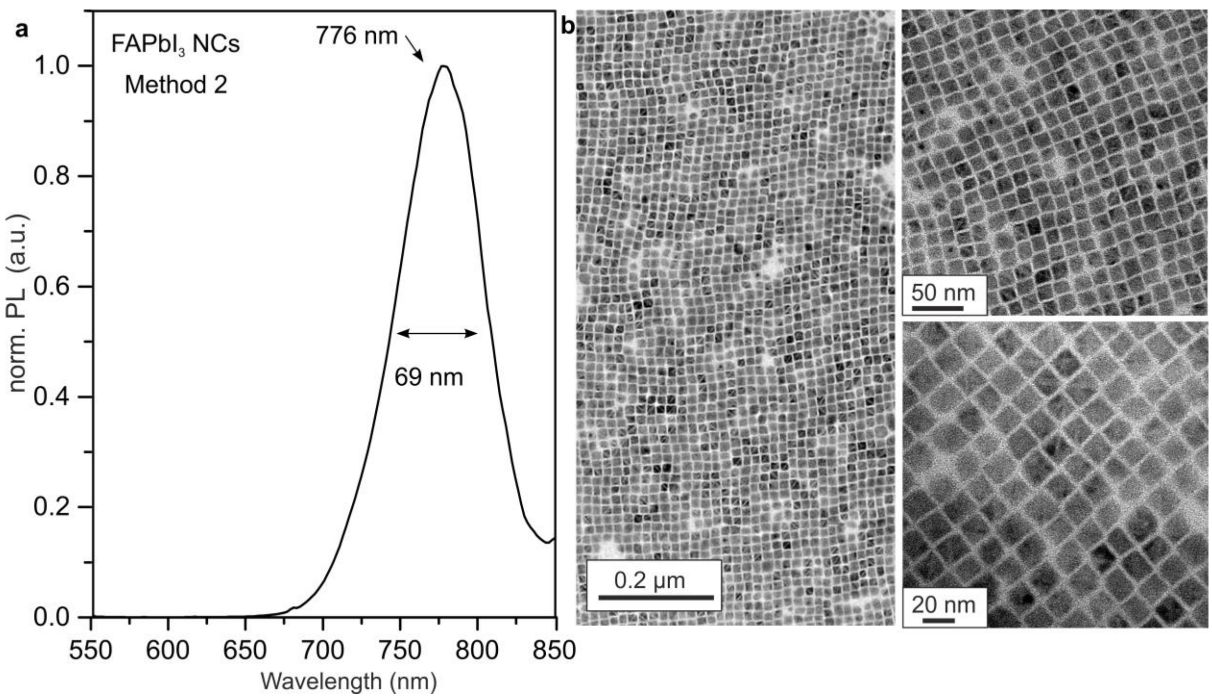

Figure S1. (a) PL spectra and (b) typical TEM images of $FAPbI_3$ NCs obtained using method 2.

The Debye Scattering Equation Method

In order to perform the structural and microstructural characterization of $FAPbI_3$ and $Cs_{0.9}FA_{0.1}PbI_3$ NCs, we adopted a Total Scattering approach based on a fast implementation of the Debye Scattering Equation (DSE), as available in the Debussy Suite.[39, 40, 41] The Debye Equation describes the differential cross section of a randomly oriented powder and allows the simultaneous modelling of the Bragg and diffuse scattering as a function of the interatomic distances within the nanoparticle:

$$I(Q) = \sum_{j=1}^{N} f_j(Q)^2 o_j^2 + 2 \sum_{j>i}^{N} f_j(Q) f_i(Q) T_j(Q) T_i(Q) o_j o_i \frac{\sin(Q d_{ij})}{(Q d_{ij})}$$

where $Q = \frac{4\pi sin\theta}{\lambda}$ is the magnitude of the scattering vector, λ is the radiation wavelength, f_{ij} is the X-ray atomic form factor, d_{ij} is the interatomic distance between atoms i and j, N is the total number of atoms and T and o are the thermal atomic displacement parameter and site occupancy factor associated to each atomic species, respectively. The first summation in the above equation includes the contributions of the zero distance between one atom and itself and the second term (the interference term) the nonzero interatomic distances $d_{ij} = | r_i - r_j |$.

The approach used in this work is the one implemented in the *DebUsSy* Suite of programs,[41] which makes use of the sampled interatomic distances instead of the original ones in order to speed up calculations.

The DSE modelling strategy used in this work can be summarized, as follows:

i) A bottom up approach was used to generate the bivariate population of atomistic models of NCs, by stacking the cubic unit cell of the α-$FAPbI_3$ phase (SG. *Pm-3m*) according to two independent growth directions, one along the *c*-axis and the other one parallel to the *ab*-plane. The cubic unit cell corresponded to the perovskite framework made by PbI_6 units, with the I anions disordered in four equivalent positions (with Pb-I-Pb bond angles deviating from their ideal 180° by *ca*. 13°) and FA^+ cations disordered between 6 sites inside the cuboctahedral cavities. This unit cell was used as the building block for generating the atomistic models of the entire population of NCs.[42] For $FA_{0.1}Cs_{0.9}PbI_3$ an orthorhombic γ-phase (SG. *Pbnm*), refined from the experimental data and isostructural to the one reported for $CsPbBr_3$,[10] was adopted. The outer organic oleate shell, nearly invisible to X-ray, has been neglected in our atomistic models.

ii) The sampled interatomic distances of the NCs were computed and stored in suitable databases, in order to calculate the DSE model pattern, used in the next step.

iii) The refinement of the model pattern against the experimental data, involving a number of adjustable parameters, was performed. To account for the size and shape distribution of $FAPbI_3$ and $FA_{0.1}Cs_{0.9}PbI_3$ NCs, we used a bivariate log-normal function with four adjustable parameters (the average and standard deviation parameters for the distribution along the two growth directions). The thermal displacement parameters were refined for all the atoms.

The graphical outcomes of the DSE analysis on $FAPbI_3$ are summarized in Figure 2 and Figure S2, for $FA_{0.1}Cs_{0.9}PbI_3$ in Figure 4 and Figure S3.

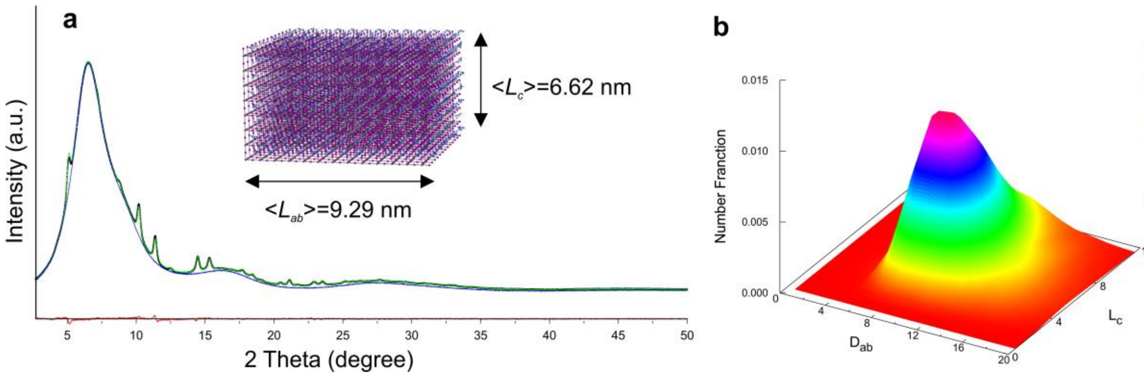

Figure S2. (a) Synchrotron XRD data of $FAPbI_3$ NCs and DSE best fit (2θ range 3-50°; λ=0.565483 Å): model pattern (green line) with its solvent component (toluene, blue line) and residual between experimental and model patterns (red line); Goodness of fit = 1.81. Inset: atomistic model of a single nanocrystal representing the average size of the sample ($<L_{ab}>$ is the length along a axis, equal to that along the b axis in our model, $<L_c>$ is the length along the c axis). (b) 3D (smoothed) map of the number-based bivariate lognormal size distribution in the $<L_c>$ and $<D_{ab}>$ coordinates ($<L_c>$ is the average size along the c axis, $<D_{ab}>$ is the diameter of the circle of equivalent area in the ab-plane). DSE estimated number-based average sizes and corresponding standard deviations σ: i) Diameter of the sphere of equivalent volume $<D_{eq}>$ = 10.06 nm; $\sigma/<D_{eq}>$ = 0.22 nm. ii) Average sizes along the two growth directions: $<D_{ab}>$ = 10.48 nm; $\sigma/<D_{ab}>$ = 0.28; $<L_c>$ = 6. Average 62 nm; $\sigma/<L_c>$ =0.35.

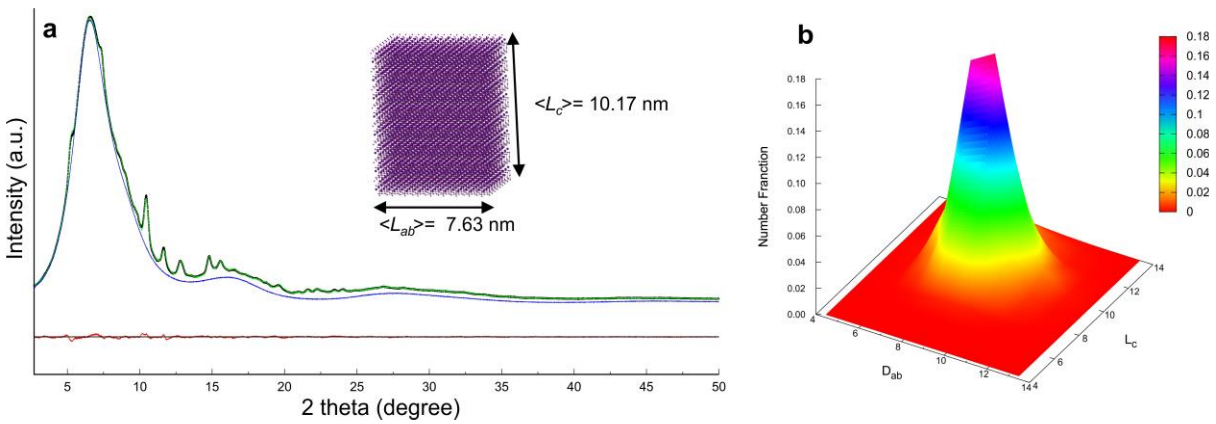

Figure S3. (a) Synchrotron XRD data of $FA_{0.1}Cs_{0.9}PbI_3$ NCs and DSE best fits (2θ range 3-50°; λ=0.565483 Å). Total model pattern (green line) with its solvent component (toluene, blue line) and residual between experimental and model patterns (red line); Goodness of fit = 1.46. Inset: atomistic model of a single NC representing the average size of the sample as in S2. (b) 3D (smoothed) map of the lognormal size distribution as in S2. DSE estimated number-based average sizes and corresponding standard deviations σ: i) Diameter of the sphere of equivalent volume: $<D_{eq}>$ = 10.39 nm; $\sigma/<D_{eq}>$ = 0.086 nm. ii) Average sizes along the two growth directions: $<D_{ab}>$ = 8.61 nm; $\sigma<D_{ab}>$= 0.12; $<L_c>$ = 10.17 nm; $\sigma/<L_c>$ = 0.11.

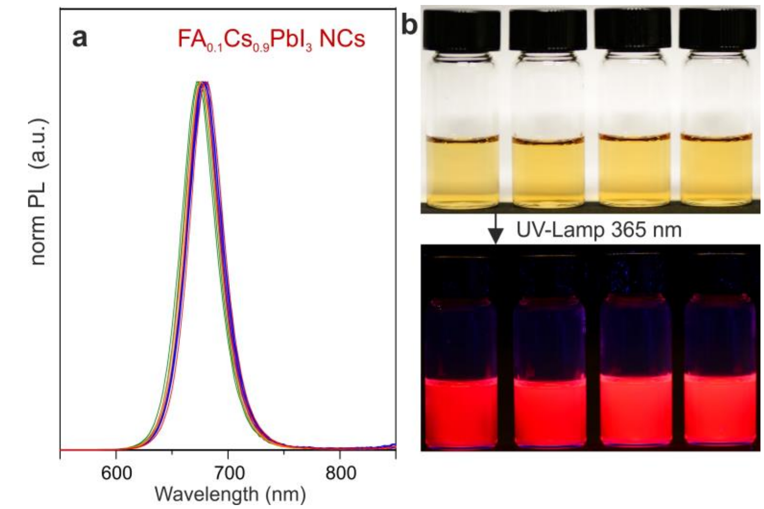

Figure S4. (a) Photoluminescence spectra for $FA_xCs_{1-x}PbI_3$ NCs obtained using various FA:Cs molar ratios of 1:1, 2:1, 1:2, 6:1 during the synthesis. (b) Photograph of the corresponding $FA_xCs_{1-x}PbI_3$ NCs dispersed in toluene under visible light and under UV light (365 nm).

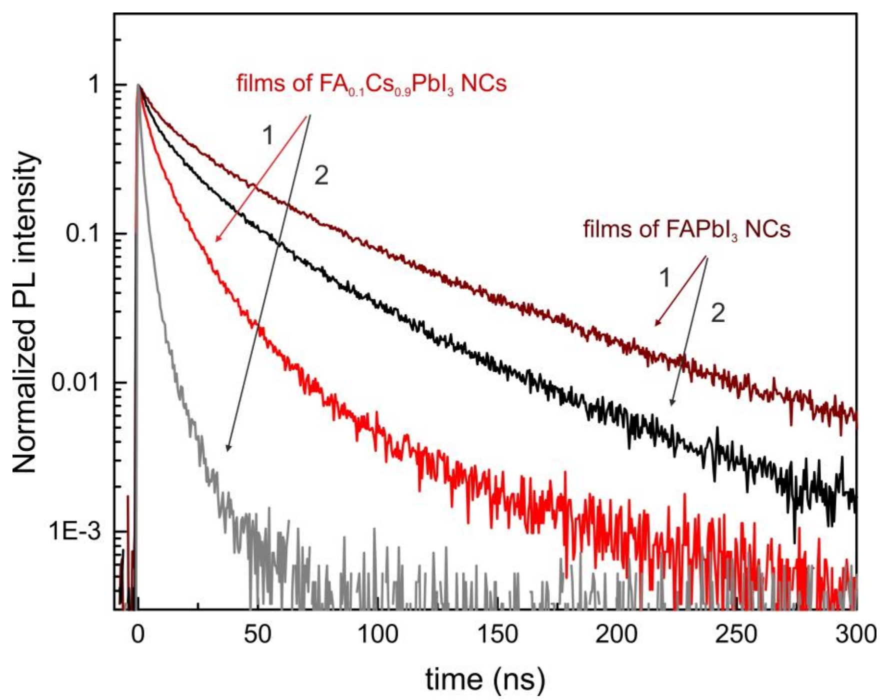

Figure S5. Time-resolved PL traces for the films of $FA_{0.1}Cs_{0.9}PbI_3$ NCs and $FAPbI_3$ NCs: (1) NCs washed with toluene only: $t_{1/e}$=50 ns $FAPbI_3$ and $t_{1/e}$ =13 ns for $FA_{0.1}Cs_{0.9}PbI_3$; (2) NCs washed once with acetonitrile (w1): $t_{1/e}$=32 ns for $FAPbI_3$ and $t_{1/e}$=5 ns for $FA_{0.1}Cs_{0.9}PbI_3$ NCs.

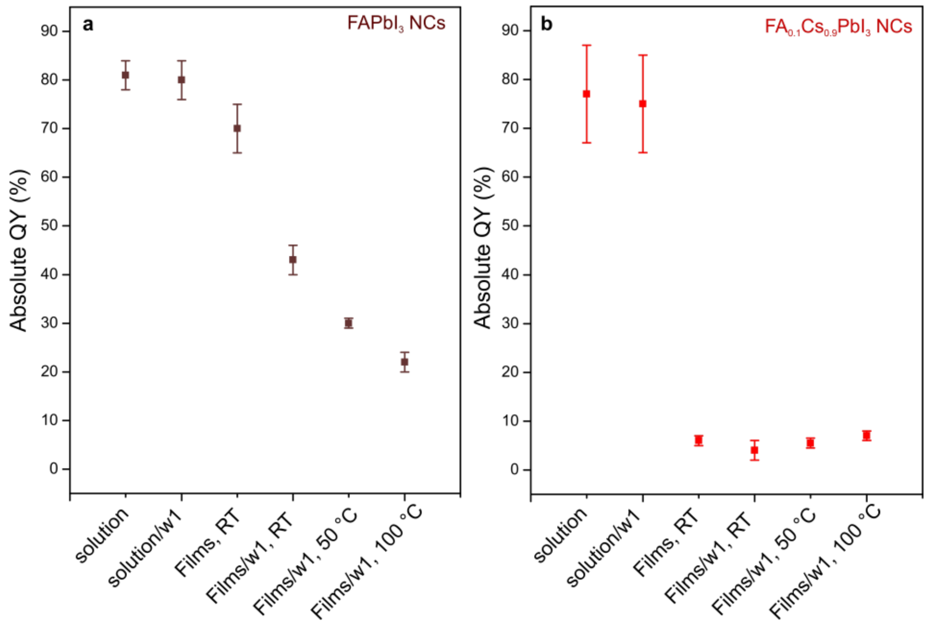

Figure S6. Absolute QY shown for (a) $FAPbI_3$ NCs and (b) $FA_{0.1}Cs_{0.9}PbI_3$ NCs measured under different conditions: colloidal solutions washed with toluene/hexane, colloidal solutions washed once with acetonitrile (w1), drop-cast films prepared from the solutions washed with toluene/hexane without heat treatment, drop-cast films prepared from solution washed once with acetonitrile (w1) without heat treatment, and after annealing at 50 °C and 100 °C for 1 h.

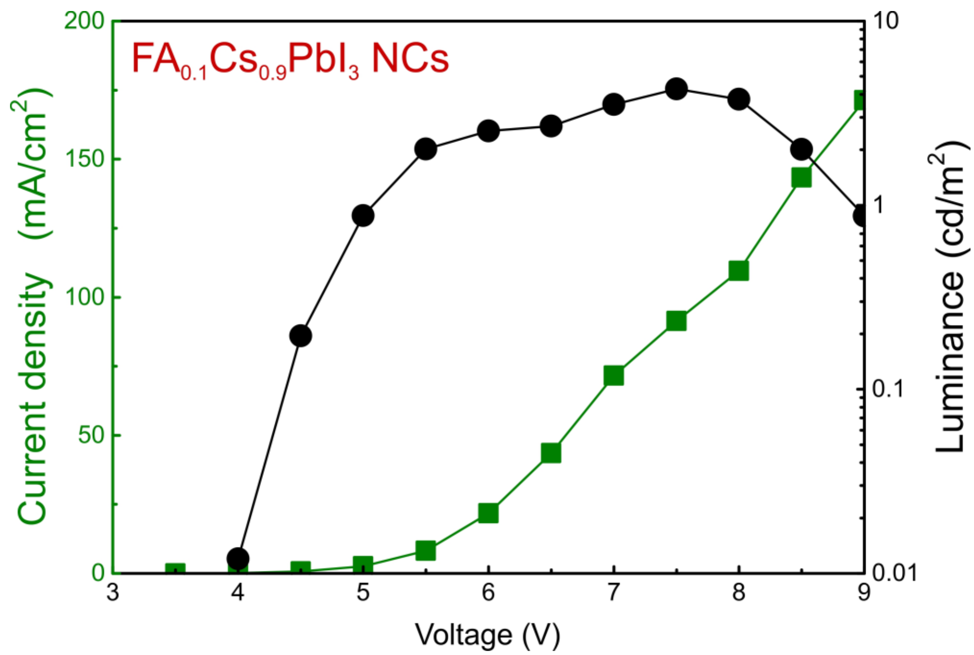

Figure S7. Current density and luminance over voltage for the LED prepared from $FA_{0.1}Cs_{0.9}PbI_3$ NCs.

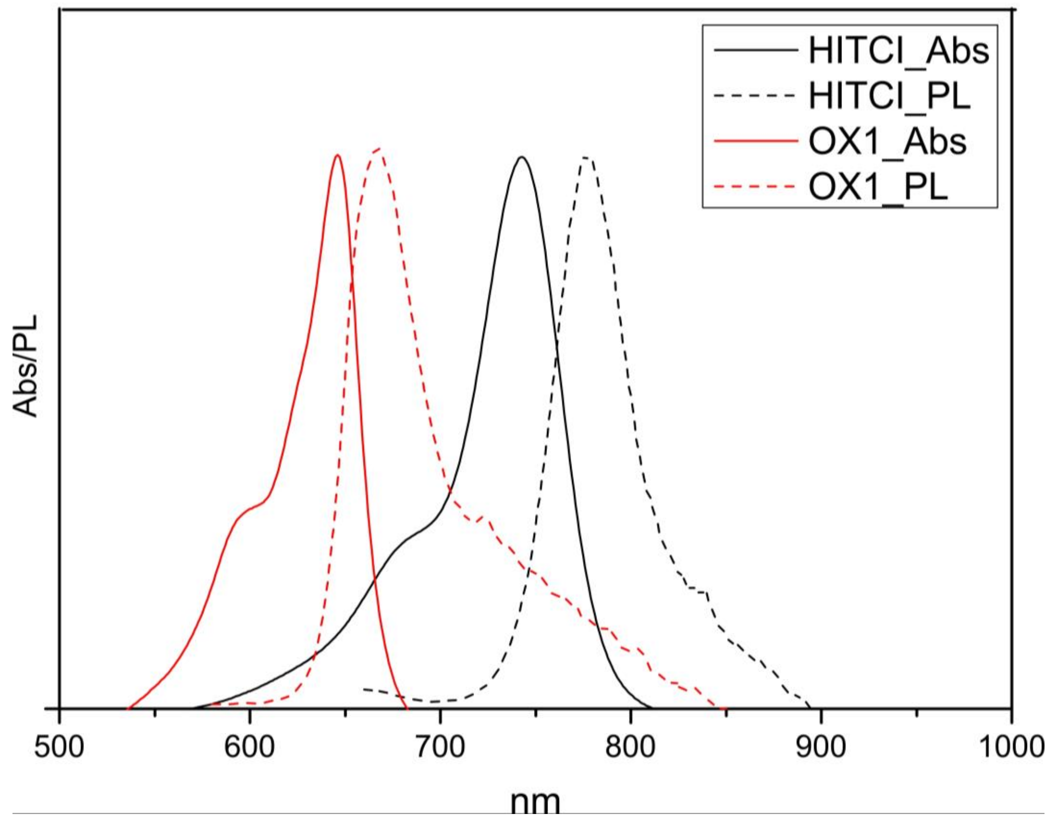

Figure S8. The photoluminescence and absorption spectra for the dyes used as references to measure the QY of $FA_{0.1}Cs_{0.9}PbI_3$ NCs (Oxine 1, OX1) and $FAPbI_3$ NCs (HITCI).[43, 44]

Supporting References:

1. Saidaminov, M. I.; Abdelhady, A. L.; Maculan, G.; Bakr, O. M., Retrograde Solubility of Formamidinium and Methylammonium Lead Halide Perovskites Enabling Rapid Single Crystal Growth. *Chem. Commun.* **2015,** *51*, 17658-17661.
2. Fang, H.-H.; Wang, F.; Adjokatse, S.; Zhao, N.; Loi, M. A., Photoluminescence Enhancement in Formamidinium Lead Iodide Thin Films. *Adv. Funct. Mater.* **2016,** *26*, 4653-4659.
3. Sharma, S.; Weiden, N.; Weiss, A., Phase-Diagrams of Quasi-Binary Systems of the Type - ABX_3-$A'BX_3$ ABX_3-$AB'X_3$, and ABX_3-ABX'_3 X = Halogen. *Z. Phys. Chem.* **1992,** *175*, 63-80.
4. Trots, D. M.; Myagkota, S. V., High-Temperature Structural Evolution of Caesium and Rubidium Triiodoplumbates. *J. Phys. Chem. Solids* **2008,** *69*, 2520-2526.
5. Stoumpos, C. C.; Malliakas, C. D.; Kanatzidis, M. G., Semiconducting Tin and Lead Iodide Perovskites with Organic Cations: Phase Transitions, High Mobilities, and Near-Infrared Photoluminescent Properties. *Inorg. Chem.* **2013,** *52*, 9019-9038.

6. Babin, V.; Fabeni, P.; Nikl, M.; Nitsch, K.; Pazzi, G. P.; Zazubovich, S., Luminescent $CsPbI_3$ and Cs_4PbI_6 Aggregates in Annealed CsI: Pb Crystals. *Phys. Status Solidi B-Basic Research* **2001,** *226*, 419-428.
7. Zhumekenov, A. A.; Saidaminov, M. I.; Haque, M. A.; Alarousu, E.; Sarmah, S. P.; Murali, B.; Dursun, I.; Miao, X.-H.; Abdelhady, A. L.; Wu, T.; Mohammed, O. F.; Bakr, O. M., Formamidinium Lead Halide Perovskite Crystals with Unprecedented Long Carrier Dynamics and Diffusion Length. *ACS Energy Lett.* **2016,** *1*, 32-37.
8. Swarnkar, A.; Marshall, A. R.; Sanehira, E. M.; Chernomordik, B. D.; Moore, D. T.; Christians, J. A.; Chakrabarti, T.; Luther, J. M., Quantum Dot–Induced Phase Stabilization of α-$CsPbI_3$ Perovskite for High-Efficiency Photovoltaics. *Science* **2016,** *354*, 92-95.
9. Heidrich, K.; Künzel, H.; Treusch, J., Optical Properties and Electronic Structure of $CsPbCl_3$ and $CsPbBr_3$. *Solid State Commun.* **1978,** *25*, 887-889.
10. Stoumpos, C. C.; Malliakas, C. D.; Peters, J. A.; Liu, Z.; Sebastian, M.; Im, J.; Chasapis, T. C.; Wibowo, A. C.; Chung, D. Y.; Freeman, A. J.; Wessels, B. W.; Kanatzidis, M. G., Crystal Growth of the Perovskite Semiconductor $CsPbBr_3$: A New Material for High-Energy Radiation Detection. *Cryst. Growth Des.* **2013,** *13*, 2722-2727.
11. Sakudo, T.; Unoki, H.; Fujii, Y.; Kobayashi, J.; Yamada, M., A New Structural Phase Transition in $CsPbCl_3$. *Phys. Lett. A* **1969,** *28*, 542-543.
12. Cohen, M. I.; Young, K. F.; Chang, T. T.; Brower, W. S., Phase Transitions in $CsPbCl_3$. *J. Appl. Phys.* **1971,** *42*, 5267-5272.
13. Saparov, B.; Mitzi, D. B., Organic–Inorganic Perovskites: Structural Versatility for Functional Materials Design. *Chem. Rev.* **2016,** *116*, 4558-4596.
14. Butler, K. T.; Svane, K.; Kieslich, G.; Cheetham, A. K.; Walsh, A., Microscopic Origin of Entropy-Driven Polymorphism in Hybrid Organic-Inorganic Perovskite Materials. *Phys. Rev. B* **2016,** *94*, 180103.
15. Maculan, G.; Sheikh, A. D.; Abdelhady, A. L.; Saidaminov, M. I.; Haque, M. A.; Murali, B.; Alarousu, E.; Mohammed, O. F.; Wu, T.; Bakr, O. M., $CH_3NH_3PbCl_3$ Single Crystals: Inverse Temperature Crystallization and Visible-Blind UV-Photodetector. *J. Phys. Chem. Lett.* **2015,** *6*, 3781-3786.
16. Hanusch, F. C.; Wiesenmayer, E.; Mankel, E.; Binek, A.; Angloher, P.; Fraunhofer, C.; Giesbrecht, N.; Feckl, J. M.; Jaegermann, W.; Johrendt, D.; Bein, T.; Docampo, P., Efficient Planar Heterojunction Perovskite Solar Cells Based on Formamidinium Lead Bromide. *J. Phys. Chem. Lett.* **2014,** *5*, 2791-2795.
17. Rehman, W.; Milot, R. L.; Eperon, G. E.; Wehrenfennig, C.; Boland, J. L.; Snaith, H. J.; Johnston, M. B.; Herz, L. M., Charge-Carrier Dynamics and Mobilities in Formamidinium Lead Mixed-Halide Perovskites. *Adv. Mater.* **2015,** *27*, 7938-7944.
18. Aygüler, M. F.; Weber, M. D.; Puscher, B. M. D.; Medina, D. D.; Docampo, P.; Costa, R. D., Light-Emitting Electrochemical Cells Based on Hybrid Lead Halide Perovskite Nanoparticles. *J. Phys.l Chem. C* **2015,** *119*, 12047-12054.
19. Wang, J.; Peng, J.; Sun, Y.; Liu, X.; Chen, Y.; Liang, Z., $FAPbCl_3$ Perovskite as Alternative Interfacial Layer for Highly Efficient and Stable Polymer Solar Cells. *Adv. Electron. Mater.* **2016,** *2*, 1600329.
20. Jang, D. M.; Kim, D. H.; Park, K.; Park, J.; Lee, J. W.; Song, J. K., Ultrasound Synthesis of Lead Halide Perovskite Nanocrystals. *J. Mater. Chem. C* **2016,** *4*, 10625-10629.
21. Chung, I.; Song, J.-H.; Im, J.; Androulakis, J.; Malliakas, C. D.; Li, H.; Freeman, A. J.; Kenney, J. T.; Kanatzidis, M. G., $CsSnI_3$: Semiconductor or Metal? High Electrical

Conductivity and Strong Near-Infrared Photoluminescence from a Single Material. High Hole Mobility and Phase-Transitions. *J. Am. Chem. Soc.* **2012,** *134*, 8579-8587.
22. Yamada, K.; Funabiki, S.; Horimoto, H.; Matsui, T.; Okuda, T.; Ichiba, S., Structural Phase-Transitions of the Polymorphs of $CsSnI_3$ by means of Rietveld Analysis of the X-Ray-Diffractions. *Chem. Lett.* **1991**, 801-804.
23. Scaife, D. E.; Weller, P. F.; Fisher, W. G., Crystal Preparation and Properties of Cesium Tin(II) Trihalides. *J.Solid State Chem.* **1974,** *9*, 308-314.
24. Donaldson, J. D.; Silver, J.; Hadjiminolis, S.; Ross, S. D., Effects of the Presence of Valence-Shell Non-Bonding Electron Pairs on the Properties and Structures of Caesium Tin(II) Bromides and of Related Antimony and Tellurium Compounds. *Dalton Trans.* **1975**, 1500-1506.
25. Shen, Z. X.; Loo, W. L.; Kuok, M. H.; Tang, S. H., High Pressure Phase Transition Studies of $CsSnCl_3$. *J. Mol. Struct.* **1994,** *326*, 73-80.
26. Kuok, M. H., Raman Study of the Phase Transition in $CsSnCl_3$. *J. Raman Spectrosc.* **1992,** *23*, 225-227.
27. Mitzi, D. B.; Feild, C. A.; Schlesinger, Z.; Laibowitz, R. B., Transport, Optical, and Magnetic-Properties of the Conducting Halide Perovskite $CH_3NH_3SnI_3$. *J. Solid State Chem.* **1995,** *114*, 159-163.
28. Yokoyama, T.; Cao, D. H.; Stoumpos, C. C.; Song, T.-B.; Sato, Y.; Aramaki, S.; Kanatzidis, M. G., Overcoming Short-Circuit in Lead-Free CH_3NH_3SnI3 Perovskite Solar Cells via Kinetically Controlled Gas–Solid Reaction Film Fabrication Process. *J. Phys. Chem. Lett.* **2016,** *7*, 776-782.
29. Swainson, I.; Chi, L. S.; Her, J. H.; Cranswick, L.; Stephens, P.; Winkler, B.; Wilson, D. J.; Milman, V., Orientational Ordering, Tilting and Lone-Pair Activity in the Perovskite Methylammonium Tin Bromide, $CH_3NH_3SnBr_3$. *Acta Crystallogr. Sect. B-Structural Science* **2010,** *66*, 422-429.
30. Chiarella, F.; Zappettini, A.; Licci, F.; Borriello, I.; Cantele, G.; Ninno, D.; Cassinese, A.; Vaglio, R., Combined Experimental and Theoretical Investigation of Optical, Structural, and Electronic Properties of $CH_3NH_3SnX_3$ Thin Films (X=Cl, Br). *Phys. Rev. B* **2008,** *77*, 045129.
31. Wang, L.-Z.; Zhao, Y.-Q.; Liu, B.; Wu, L.-J.; Cai, M.-Q., First-Principles Study of Photovoltaics and Carrier Mobility for Non-Toxic Halide Perovskite $CH_3NH_3SnCl_3$: Theoretical Prediction. *Phys. Chem. Chem. Phys.* **2016,** *18*, 22188-22195.
32. Lee, S. J.; Shin, S. S.; Kim, Y. C.; Kim, D.; Ahn, T. K.; Noh, J. H.; Seo, J.; Seok, S. I., Fabrication of Efficient Formamidinium Tin Iodide Perovskite Solar Cells through SnF_2–Pyrazine Complex. *J. Am. Chem. Soc.* **2016,** *138*, 3974-3977.
33. Koh, T. M.; Krishnamoorthy, T.; Yantara, N.; Shi, C.; Leong, W. L.; Boix, P. P.; Grimsdale, A. C.; Mhaisalkar, S. G.; Mathews, N., Formamidinium Tin-Based Perovskite with Low Eg for Photovoltaic Applications. *J. Mater. Chem. A* **2015,** *3*, 14996-15000.
34. Shannon, R. D., Revised Effective Ionic-Radii and Systematic Studies of Interatomic Distances in Halide and Chalcogenides. *Acta Crystallogr. Sect. A* **1976,** *32*, 751-767.
35. Travis, W.; Glover, E. N. K.; Bronstein, H.; Scanlon, D. O.; Palgrave, R. G., On the Application of the Tolerance Factor to Inorganic and Hybrid Halide Perovskites: a Revised System. *Chem. Sci.* **2016,** *7*, 4548-4556.
36. Vybornyi, O.; Yakunin, S.; Kovalenko, M. V., Polar-Solvent-Free Colloidal Synthesis of Highly Luminescent Alkylammonium Lead Halide Perovskite Nanocrystals. *Nanoscale* **2016,** *8*, 6278-6283.

37. Dirin, D. N.; Protesescu, L.; Trummer, D.; Kochetygov, I. V.; Yakunin, S.; Krumeich, F.; Stadie, N. P.; Kovalenko, M. V., Harnessing Defect-Tolerance at the Nanoscale: Highly Luminescent Lead Halide Perovskite Nanocrystals in Mesoporous Silica Matrixes. *Nano Lett.* **2016,** *16*, 5866-5874.
38. Protesescu, L.; Yakunin, S.; Bodnarchuk, M. I.; Krieg, F.; Caputo, R.; Hendon, C. H.; Yang, R. X.; Walsh, A.; Kovalenko, M. V., Nanocrystals of Cesium Lead Halide Perovskites ($CsPbX_3$, X = Cl, Br, and I): Novel Optoelectronic Materials Showing Bright Emission with Wide Color Gamut. *Nano Lett.* **2015,** *15*, 3692-3696.
39. Debye, P., X-ray Dispersal. *Ann. Phys.* **1915,** *46*, 809-823.
40. Cervellino, A.; Giannini, C.; Guagliardi, A., On the Efficient Evaluation of Fourier Patterns for Nanoparticles and Clusters. *J. Comput. Chem.* **2006,** *27*, 995-1008.
41. Cervellino, A.; Frison, R.; Bertolotti, F.; Guagliardi, A., DEBUSSY 2.0: TheNew Release of a Debye User System for Nanocrystalline and/or Disordered Materials. *J. Appl. Crystallogr.* **2015,** *48*, 2026-2032.
42. Weller, M. T.; Weber, O. J.; Frost, J. M.; Walsh, A., Cubic Perovskite Structure of Black Formamidinium Lead Iodide, α-$[HC(NH_2)_2]PbI_3$, at 298 K. *J. Phys. Chem. Lett.* **2015,** *6*, 3209-3212.
43. Grabolle, M.; Spieles, M.; Lesnyak, V.; Gaponik, N.; Eychmüller, A.; Resch-Genger, U., Determination of the Fluorescence Quantum Yield of Quantum Dots: Suitable Procedures and Achievable Uncertainties. *Anal. Chem.* **2009,** *81*, 6285-6294.
44. Rurack, K.; Spieles, M., Fluorescence Quantum Yields of a Series of Red and Near-Infrared Dyes Emitting at 600−1000 nm. *Anal. Chem.* **2011,** *83*, 1232-1242.